Mesoscale Modeling of Tension Analysis of Pure and Intra-ply Hybrid Woven Composites Using Finite Element Method

Majid Tehrani Dehkordi

Abstract— **One of the key issues associated with using of composites in various applications is their tensile behavior. The tensile behavior of a composite material is strongly influenced by the properties of its constituents and their distribution. This paper focuses on gaining some insights into the tensile process of pure and hybrid woven composite reinforced with brittle and ductile yarns. For this purpose, mesoscale finite element simulations were performed to detect the tensile response within three types of composites: i.e, a brittle fiber reinforced composite, a ductile fiber reinforced composite and a brittle/ductile fiber reinforced composite. The numerical predictions were then compared with the experimental observations and the results were discussed to give some insights into the reinforcing mechanisms in the composites. Based on the results it can be concluded that this finite element model is a reliable tool in the prediction of the tensile behavior of pure and hybrid composite materials.**

Keywords: Mesoscale modeling, finite element method, brittle fiber, ductile fiber, tensile properties, composite.

I. INTRODUCTION

Fiber reinforced composites are made by combining two or more constituents to form a solid material and are designed to take the benefits from the constituent phases. Many different reinforcements are used to make composites including brittle and ductile fibers [1, 2]. The results of the previous studies have indicated that brittle fiber reinforced composites lose their tensile strength immediately after first cracking under uniaxial tension and is no longer able to resist any stress [3]. To compensate the defects of brittle reinforced composite, hybrid composites have been designed [4, 5]. Hybrid composites contain more than one type of fiber in a single matrix material [5].

M. Tehrani Dehkordi with the Department of Carpet, Shahrekord University, Shahrekord, Iran. Correspondence should be addressed to M. Tehrani Dehkordi (e-mail: mtehrani@lit.sku.ac.ir).

Experimental techniques can be employed to understand the effects of various fibers and matrix properties in hybrid composites. These experiments require fabrication of various composites with the above mentioned parameters, which are time consuming and cost prohibitive. Therefore, a computational model is used which can be easily altered to model hybrid composites with different constituents; hence saving the designer's valuable time and resources. In the early stages of computer age, finite element (FE) codes were rapidly implemented to simulate the mechanical behaviour of structures, providing more accurate insight on this subject [6-8]. FE method has successfully been used in analysis and designing of composite materials and composite structures. Many researches have been published using FE methods to model the elastic and elastic-plastic (non-linear) behavior of composites. The elastic behavior of composites has been examined by many researchers [9-13]. Several researchers have investigated the elastic-plastic behavior of fiber reinforced composites. Three different approaches have been used: micro-scale, mesoscale and macro-scale approaches. The macro-scale model is to get the overall properties of desired composite structure by extracting the results from mesoscale model. Although this approach is usually simpler, it often relies heavily on experimental data [14-17]. The mesoscale model focuses on the study of the overall property of composite unit cell by introducing of geometry of unit cell and considering yarns and matrix as homogeneous materials. The overall property of homogeneous yarn is calculated from micro-mechanical model. Finally, the micro-scale model studies the property of composite reinforcement by taking into account the orientation, structure and properties of constituent fibers. This model is actually transfers the properties of constituent fibers to overall property of the yarn assemble. The micro or mesoscale approaches allow modeling more complicated composite behavior and reducing tests needed by taking interaction into account. A few micro-scale and mesoscale FE works exist on non-linear behavior of composites. Several authors such as Christensen et al. [18], Adams and Crane [19], Parietti [20], Briancon et al. [21], Zhao et al.

[22], Zhang et al. [23], Vogler et al. [24] and Grujicic et al. [25] used the FE method to study the response of a representative volume element (RVE) of a composite lamina. These models are established with the matrix described by a nonlinear elastic-plastic model and the fiber by an elastic one. In another study, Zhang [26] used a multi scale nonlinear FE modeling technique to predict the progressive failure process for composite laminates. Tabiei et al. [27] developed a micromechanical model for composite material of woven fabrics including the nonlinear stress-strain behavior. They coded a user defined subroutine in the Abaqus finite element package to define the constitutive behavior of woven fabrics including the nonlinearity.

One of the key issues associated with the use of composites is their tensile behavior. Even though overall tensile behavior of composite reinforced with elastic fiber is reasonably well understood, composite reinforced with brittle and ductile fiber have not been investigated. This paper focuses on gaining some insight in the tensile behavior of pure and hybrid woven composite reinforced with brittle and ductile yarns. For this purpose, mesoscale FE simulations were performed to detect the tensile response within the three types of composites: a brittle fiber reinforced composite (pure basalt), a ductile fiber reinforced composite (pure nylon) and a brittle/ductile fiber reinforced composite (basalt/nylon intra-ply hybrid). The numerical predictions were then compared with the experimental observations and the results were discussed to give some insights into the reinforcing mechanisms of the composites.

II. Experimental and Method

In the present study, a mesoscale model for tension analysis of pure and hybrid composites is proposed. The meso model of composites required some characteristics of their constituents such as density, elastic modulus and poisson's ratio. These characteristics were obtained using experimental tensile test and manufacturers' data and are listed in Table I.

TABLE I
PROPERTIES OF VARIOUS CONSTITUENTS

Property	Basalt fiber	Nylon fiber	Epoxy
Density (Kg/m^3)	2700	1250	1110
Young's modulus (GPa)	76	2.45	2.73
Poisson's ratio	0.23	0.26	0.35
Maximum principle strain (%)	1.9	20.5	3.6

To evaluate the proposed model, three types of fabric-reinforced composites were produced, namely pure basalt, pure nylon and basalt-nylon intra-ply hybrid composites. The basalt and nylon yarns were supplied by Gold Basalt Fiber Co. (China) and Junma Tyre Cord Co. (China) with the counts of 800 Tex and 365 Tex, respectively. The structure of the woven fabric reinforcements is shown in Figure 1. In this Figure, the black color represents basalt yarns and the white color represents nylon yarns. The fabric counts in the warp and weft directions were 5 ends/cm and 5 picks/cm. These specimens were prepared from a composite with plain fabric reinforcement in thermo-set epoxy polymer matrix. All of the composites had the same fiber volume fraction (about 60%) in the warp and weft directions. The volume fractions of the fibers in each direction and the matrix were estimated based on the yarn sizes, fiber specific densities; perform constructions, and composite specific densities [5].

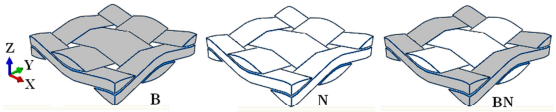

Fig. 1. Structure of the fabrics used in this study. (B) pure basalt, (N) pure nylon and (BN) 50% basalt and 50% nylon.

The prepared composites were used to measure the tensile properties according to ASTMD.3039 [28]. The tests were carried out on rectangular specimens of 250 mm length and 25 mm width along the X direction in Figure 1. For calculating the tensile modulus and poisson's ratio, strain gauges were mounted on one surface of each specimen based on ASTM standards.

All the tensile tests were carried out at a cross head speed of 2 mm/min, using an Instron 8033 test machine. The distance between the grips was fixed at 100 *mm*.
During the test, a data acquisition system recorded the force versus displacement history. From the basic force–displacement information, important parameters such as stress and strain were calculated. The tensile strength (σ) values were calculated from the following equation;

$$\sigma = F/A \quad (1)$$

where, F is the ultimate load, and A is the cross sectional area of the specimen. Elastic modulus was obtained from the initial slope of stress (σ) - strain (ε) curves based on the equation below;

$$E = \sigma / \varepsilon \quad (2)$$

The experimental results obtained for various composites are summarized in Table II.

TABLE II
TENSIL RESULTS FROM FE METHOD AND EXPERIMENT

Sample		Ultimate stress (MPa)	Elastic modulus (GPa)	Poisson's ratio
B	Theory	283	15.83	0.19
	Experiment	248	15.54	0.16
	Difference (%)	14.11	1.86	23.75
N	Theory	167	1.29	0.32
	Experiment	141	1.22	0.27
	Difference (%)	18.43	5.73	18.51
BN	Theory	112	6.06	0.26
	Experiment	90	4.89	0.23
	Difference (%)	23.33	23.92	13.04

A. *Numerical Modeling*

1) Mesoscale Modeling and Assumptions

Upon the decision to model reinforced composites on the mesoscale it is important to create appropriate RVE or unit cells. The RVE has regularly separated arrays of yarns embedded in a homogenous matrix material so that it can be isolated from the whole composite. The RVE has the same fiber volume fraction as the composite laminate and the respective properties of the yarn and matrix individually. The individual constituents are used in the RVE model in order to predict the overall response of the composite. The representative volume of a plain weave composite model is shown in Figure 2. The size of the unit cell is 4 mm, 4 mm and 0.82 mm along the X, Y and Z directions, respectively. The unit cell consists of a complete yarn and two split yarns in each principle direction and the matrix.

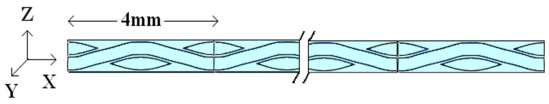

Fig. 2. The representative volume for the composite model.

As with the vast majority of modeling, certain assumptions have been made in the creation of the unit cell presented here. First, and the most important one, it has been assumed that many fibers present in the woven lamina in one direction can be considers one large fiber (yarn) in the unit cell. This means that some details in stress response will be lost but significantly reduces the computing power required to carry out the analysis. Secondly, in the model, the yarn is assumed as a continuous media but in fact, it is a porous media. Thirdly, in the presented unit cell, the voids and other irregularities were ignored. Although, the presented unit cell is very simple and entails some basic assumptions, it will be still accurate enough in understanding the type and admixture yarn effects on the tensile properties.

2) Finite element model

The numerical analysis was performed using the commercial Abaqus / Standard FE code version 6.10. Due to the simple tensile processing, the strategy adopted to model its behavior follows the main steps available in the FE package:

- Part: A three-dimensional (3D) mesoscale FE model was constructed. The model geometry consisted of a complete yarn and two split yarns in each principle direction and the matrix. The yarns and matrix parts were simulated solid and deformable, as shown in Figure 3. The yarns and the matrix were geometrically generated. The matrix model was generated with 3D extrusion element. 3D sweep elements with a racetrack cross-section were used to generate yarn parts. The yarn cross-section and geometrical parameters were obtained with considering the fabric cross-section in experimental procedure and microscopy images, as shown in Figure 4.

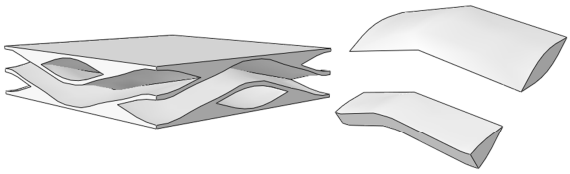

Fig. 3. Construction of matrix and yarn parts.

Fig. 4. Fabric cross-section in experimental procedure.

- Assembly: The analysis of failures at mesoscopic level requires a mesoscale model. Therefore, fully 3D FE models of yarn and matrix assemblies were adopted. Figure 5(a) shows the merge model used to simulate the tensile test. In this figure, copies of the individual parts i.e. yarns and matrix were generated and assembled to produce the unit cell of a plain weave composite. In woven

composites the warp and weft fiber bundles are positioned at 90° to each another as shown in Figure 5 (b).

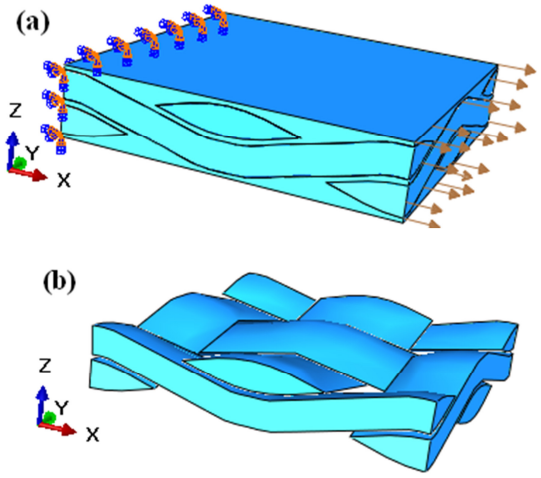

Fig. 5. (a) The merge model of composite, (b) The unit cell of woven fabric with two constituents: warp (yarn along X direction) and weft (yarn along Y direction) yarns.

• Property: The matrix part is assumed to be constituted of an elastic linear material. In fact, the epoxy resin used as matrix has a non-linear behaviour near its fracture stress [29]. However, when confined to a very small layer between adherents, epoxies show a linear elastic behaviour up to rupture [30].

The elastic and plastic material managers were set up using the isotropic properties of the fiber materials. Elastic properties and the density of various constituents were listed in Table I. In order to allow the model to handle more realistic material behaviors such as nonlinearity, it is necessary to include plasticity part. The plastic part of fibers was determined by some points in the plastic region at their load-elongation curves.

The proportions of the half and complete yarns have been varied to obtain three different composites. The composites reinforced with pure basalt (B), pure nylon (N) and admixture of 50% volume ratio of basalt and 50% volume ratio of nylon (BN) are shown in Figure 1.

Damage initiation refers to the onset of degradation at a material point. In this study, the damage initiation criteria for each constituent of fiber- reinforced composites are based on maximum strain theory (Maxpe Damage) [31]. In this criterion, longitudinal strain of each element in principal material coordinates must be less than the respective strain; otherwise, it is said that fracture has occurred on that element. Table I lists the maximum principle strain for the constituents used in this analysis.

• Step: The static analysis was used for solving tensile process. For obtaining the nonlinear geometric effect, the NLGEOM parameter is used on the step option.

The step module also allows the user to submit output requests. Element stress/strain and field variable status output from the analysis was requested after each increment, resulting in minimum 25 data-points for a full tensile test simulation run. This was felt to be sufficient to provide output for comparison with experimentally derived stress/strain curves.

• Interaction: The interaction module allows the user to set up interface definitions between various areas of the model. To perform the interface between yarn and matrix parts, the tie constraint type was used in the model. The yarns constrained together using surface to surface contact (standard). This constraint prevents yarns interference during the analysis.

• Boundary condition: The loading and boundary conditions for the mesoscale cells are defined based on the results of macro scale. Figure 5(a) shows the loading and boundary condition of the problem under consideration. It can be seen that one of the extremities of the joint, at the area under the grip of the tensile test machine, has the restrictions of a cantilever beam, and the other extremity acts as a simple supported beam. The uniaxial tension was applied to the simple supported extremity using uniform Velocity/Angular velocity with constant cross-head speed of 1.33×10^{-6}m/s. The numerical cross-head speed (V_n) is calculated from the following equation;

$$V_n = L_n \times V_E / L_E \quad (3)$$

Where, L_n is the length of analyzed unit cell, and L_E and V_E are the lengths of sample and cross-head speed in standard test method for tensile properties [28], respectively.

• Mesh: To determine the most appropriate mesh element for the problem, several elements were tested. After preliminary tests, eight-node hexahedral linear element (C3D8R) was chosen for yarn parts with a nominal edge length of 0.2 mm. This type of element has 3D solid and brick structure, which is shown in Figure 6(a). The FE mesh used to model the matrix part is shown in Figure 6(b). 9960 reduced integration four-node tetrahedral linear elements (C3D4R) were used, with a nominal edge length of 0.2 mm.

• Solve: The problem was solved using Abaqus standard solver.

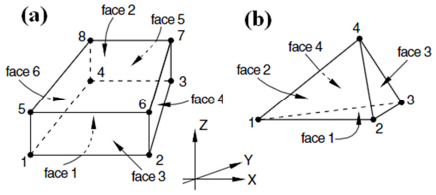

Fig. 6. (a) 8-node hexahedral element, (b) 4-node tetrahedral element [31].

III. RESULTS AND DISCUSSION

A. Comparison of Numerical and Experimental Results

In order to verify the computer model, tensile tests were performed on three types of composites and compared with predicted tensile properties. The stress/strain curves of the samples B, N and BN from the simulation and experimental tests are shown in Figure 7 (a) - (c), respectively. It was observed that stress-strain response of the all samples is non-linear. In these figures for all samples the correlation between simulation and experiment is excellent up to approximately 1% strain, where the experimental test shows a reduction in stress which is not reflected in the simulation. In the experimental test, the specimen begins to damage at low strain levels and shows a progressive reduction in stiffness. The simulation shows little reduction in stiffness up to approximately 2, 4 and 2% strain for samples B, N and BN, respectively. After this point, damage development is more rapid in the simulation than in the test and the stress rise reduces significantly.

At strain (higher than 1%) in samples B and N, the simulations show good correlation with experiments, although ultimate failure occurs later in the simulation than in the test and the stiffness of the specimen is predicted to be slightly higher as compared to when the specimen is tested.

The explanation for stress-strain response of sample BN on Figure 7(c) is much more complex and further investigation must be made to get a full understanding of the behaviour. For hybrid specimen, in which both basalt and nylon yarns are simultaneously present along the loading direction, two subsequent load drops could be detected: the first load drop was associated with the failure of the basalt fiber and the second one corresponded to the failure of the nylon fiber. Figure 7(c) shows that the form of the simulation curve is similar to that seen in the experiment tensile test. In this figure, a discrepancy between the simulation prediction and experiment can be noticed; it appears that the pattern and the stress-strain curves are show similar.

An overall tensile characteristic of investigated samples i.e. ultimate stress, elastic modulus and poisson's ratio is given in Table II both experimental and numerically calculated values.

It can be seen that the ultimate stresses obtained from simulation was slightly larger than those obtained from experimental tests, this could be due to the tie constraint between yarns and matrix and ignoring the voids in numerical model. The differences between simulation and experimental test results are about 14%, 18% and 23% for B, N and BN specimens, respectively.

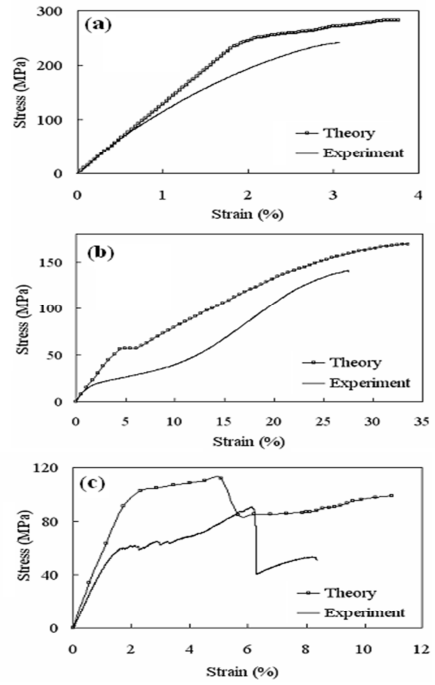

Fig. 7. Experimental and numerical stress/strain curves of various composites, (a) B, (b) N and (c) BN samples.

As a result of the non-linearity at high strains the elastic modulus of each specimen was calculated between strains of 0.3% to 0.8%. This region of the stress-strain curve was found to be linear for all three specimens and was free from initial loading effects. The elastic modulus values were calculated using the Equation (2). The results show that the experiments provided 2%-24% lower elastic modulus compared to the simulations. It was found that the axial stress in the experiment were lower than those obtained from the simulations due to the earlier damage at low strain levels of experimental tests (See Figure 7(a)-(c)).

By examining the overall longitudinal expansion and transverse contraction of the unit cell in Figure 8, the composite poisson's ratio can be derived. The poisson's ratio for the composite is defined as minus the ratio of strain in the y-direction divided by the strain in the x-direction when only the stress is applied in the x direction. The experimental and simulation poisson's ratio for all the specimens are listed in Table II. The simulation provided poisson's ratios which were around 23% (for sample B), 18% (for sample N) and 13% (for sample BN) greater than those provided by the experiment tests.

The reasons of differences between simulation and experiment results are the assumptions that made in the simulation and experimental errors. To improve the numerical results and reach the real composite model, the mentioned assumptions have to be decreased or corrected.

Considering the spread of simulations results from experiment, it is shown that the calibration for tensile characteristics is accurate and the model successfully predicts the behavior of pure and hybrid specimens in tension.

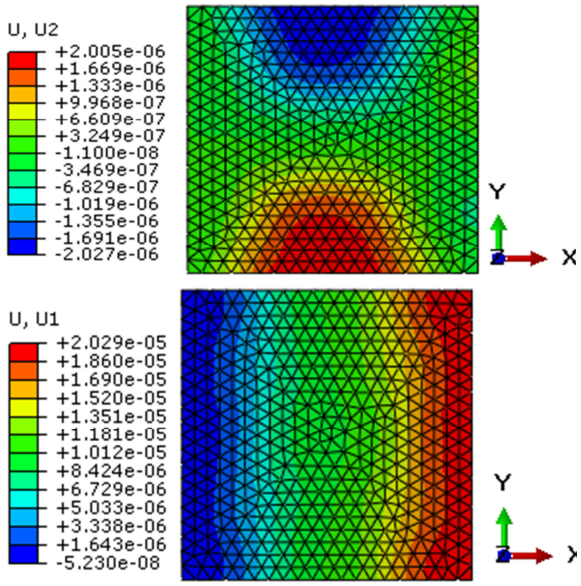

Fig. 8. Contour plots of displacement u_1 and u_2 for sample B.

B. Analysis of Stress State Within the Composite

Some parameters such as type and distribution of stress can delineate at each increment of simulation. These data are not obtained with the experimental test instruments. Some contour plots of stress for investigated specimens are presented in the following figures. These figures are used for stress analyzing and they find the susceptible parts of the composite tools.

Typically, the S_{11}, S_{22}, S_{33}, S_{12}, S_{13} and S_{23} stress contour plots of B sample are shown in Figure 9. It can be seen that the principle stress acting on the specimen is the longitudinal stress S_{11}. The range of S_{22} stresses is small and the magnitudes are lower than the longitudinal tensile stress where the maximum S_{22} (110.6 MPa) is around 2.5 times smaller than the maximum tensile S_{11} (283.8 MPa). A similar story is found for S_{33} where the maximum tensile stress S_{33} (40.93 MPa) is around 7 times smaller than the maximum tensile stress S_{11} and as a result it is not deemed to have an effect on the failure of the specimens. Similar findings are found for the induced shear stresses where the maximum values are substantially lower than the longitudinal stress value. Again, this demonstrates that the specimens should fail due to the longitudinal stress S_{11}. The stress responses of the other examined specimens (N and BN) were similar to the B specimen.

Figure 10 shows the damage build up in the constituent of the B specimen (yarns and matrix) during the simulation. Damage does not develop during the initial stages of the simulation, as the specimen is deformed elastically (Figure 10 (a)). At approximately 1% strain, damage starts to propagate progressively along the loading direction (Figure 10 (b-c)). This builds up until ultimate failure, which occurs in the specimen at approximately 3.6 % strain. This ultimate failure occurs across the width of the specimen at the middle of the weft yarns where the cross-sectional area is least (the region marked in Figure 10 (d)). The increase in the strain is due to the reduction in thickness at this region. This is known as the knee phenomenon [32].

The final damaged states of the investigated specimens are shown for test and simulation to compare the damage prediction (Figure 11). It can be observed that the damage propagation pattern is different in each specimen. In the simulation figures, ES/US is defined as the ratio of the element stress divided by the ultimate stress for each constituent.

For the B specimen, the basalt fiber begins to fail, but the matrix remains intact. Therefore, rupture occurs at all constituent of specimen suddenly without warning like brittle fracture. This mode of failure is similar to that seen during the experimental test (Figure 12(a)).

The damage contour from the N model is shown in Figure 13(a). This figure shows an uneven stress distribution and a great difference between the level of stress in the surrounding matrix and the nylon fiber, which leads to more fracture in the matrix with a little damage in nylon fiber. Predicted damage is compared to a failed experimental test specimen in Figure 12 (b). It can be seen that the shape of the failure zone is predicted accurately. The failure of the N model results in a gradual growth in damage at approximately 33% strain (Figure 13(b)). In the failure point, the constituent of N specimens (especially matrix section) destroyed completely throughout the sample. A typical experimental failed specimen is shown in Figure 12(c). This image confirms the response observed in the simulation and experimental tests.

The predicted damage in the BN specimen is shown in Figure 14. The differences in elastic properties of basalt and nylon fiber cause concentrated stress which was not uniform in constituents and the difference between the level of stress in the matrix, basalt fiber and the nylon is very high. It can be seen that the stress concentrated at the basalt fiber is 9.5 times more than the stress in the nylon fiber. In this case the matrix and basalt fiber fail, but the nylon fiber remains intact and continues to function in load bearing up to complete failure. This was seen in the experimental test, where the matrix and basalt fiber failure was only observed around the fracture zone (Figure 12(d)).

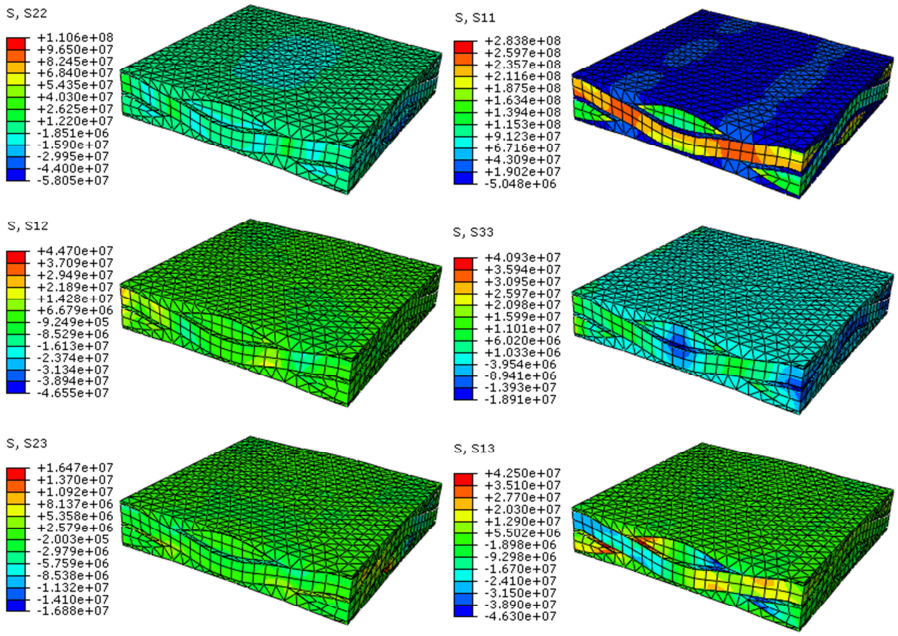

Fig. 9. Stress contour plots of the B specimen.

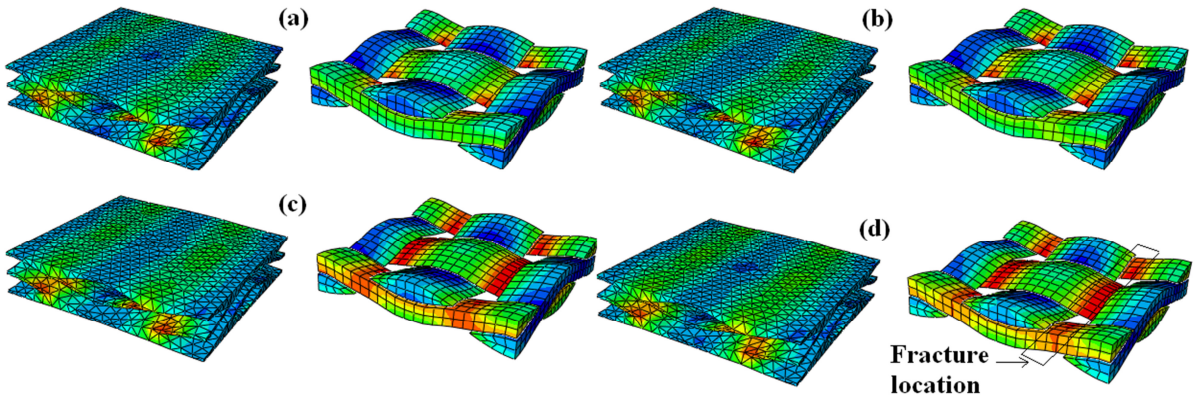

Fig. 10. The damage builds up in the constituent of the B specimen during the simulation.

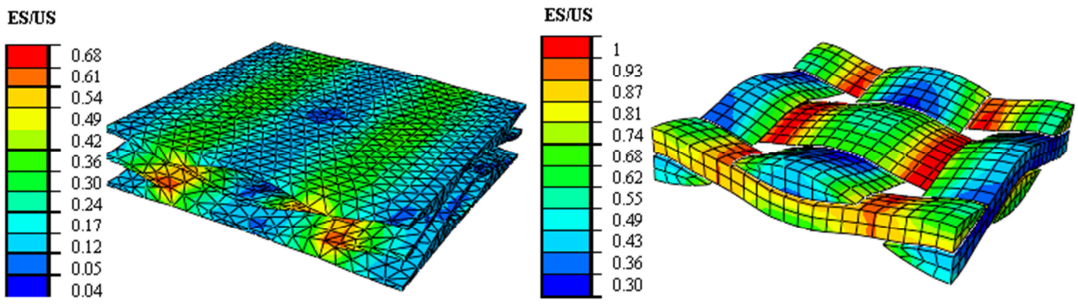

Fig. 11. Predicted damage contours of the B specimen.

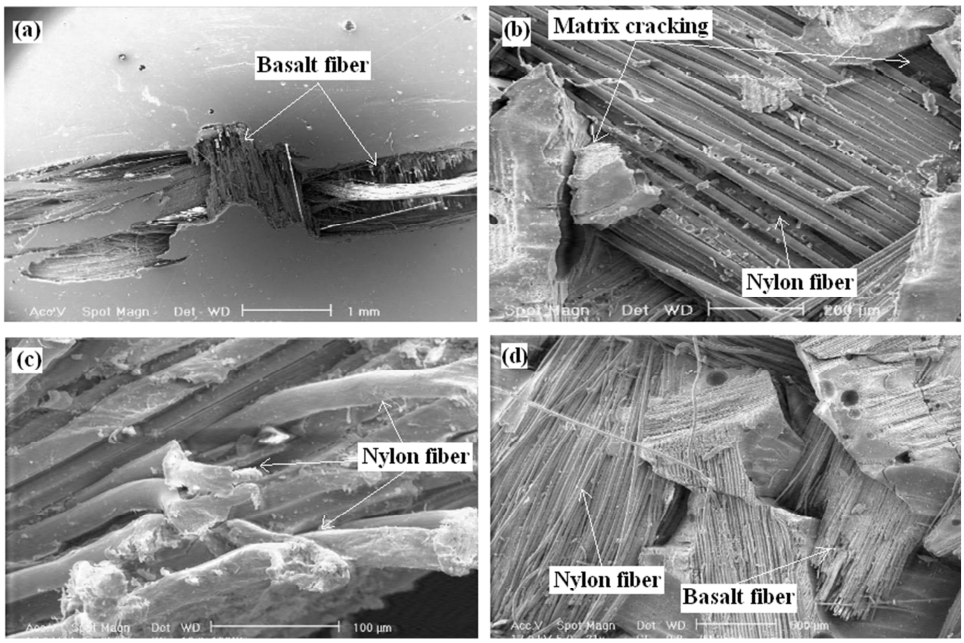

Fig. 12. Final damaged states of the investigated specimens; (a) B, (b)-(c) N, (e) BN.

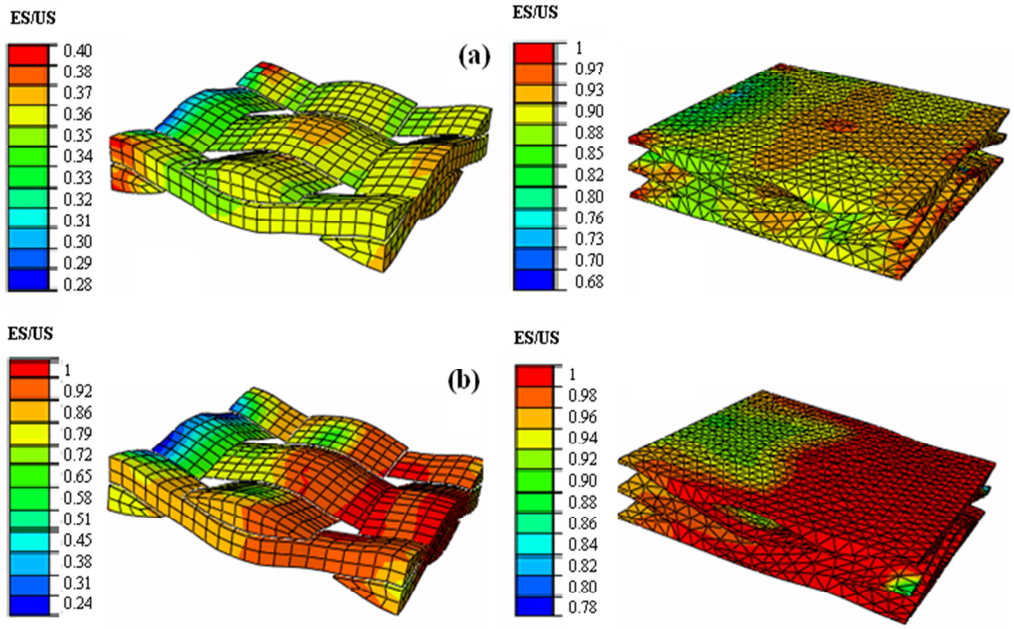

Fig. 13. Predicted damage contours of the N specimen; (a) matrix failure state, (b) final damage state

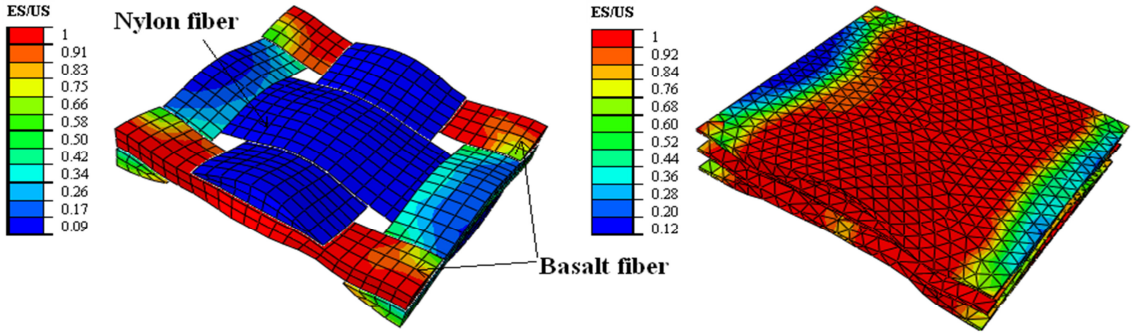

Fig. 14. Predicted damage contours of the BN specimen

IV. CONCLUSIONS

In the present study, a mesoscale FE model has been simulated to predict the tensile behaviour of pure and intra-ply hybrid composites reinforced with brittle and ductile yarns. In order to verify the computer model, tensile tests were performed on three types of composites and then were compared with predicted properties. The results showed that:

- The form of the simulation stress-strain curve is similar to that seen in the experiment tensile test. In hybrid sample, a discrepancy between the simulation prediction and experiment can be noticed; nevertheless the agreement is generally considered good. In this sample for both simulation and experiment cases, the process of fracture takes place in two sequential stages: basalt fiber fracture and nylon fiber fracture.
- The ultimate stress in the simulation investigated specimens was slightly larger than those obtained from experimental test. The differences between simulation and experimental test results are about 14%, 18% and 23% for pure basalt, pure nylon and basalt/nylon hybrid specimens, respectively.
- The model provided 2%-24% higher elastic modulus compared to the experiments.
- The simulation provided poisson's ratios were around 23% (for pure basalt), 18% (for pure nylon) and 13% (for basalt/nylon hybrid) greater than those provided by the experiment tests.
- The longitudinal stress (S_{11}) is the dominant resultant stress in the specimens.
- The final damaged states show that the damage propagation pattern is different in various investigated specimens. The uneven stress distributions in the pure specimen models (B and N model) are lower than the hybrid laminate model.

Acknowledgments

The work described in this paper was supported by a grant from the Research Committee of Shahrekord University.

REFERENCES

[1] L. F. Thompson, "Through-thickness compression testing and theory of carbon fibre composite materials", PhD Thesis, University of Manchester, 2011.

[2] M. Nasr-Isfahani, M. Latifi, M. Amani-Tehran, L. Warnet and M. Halvaei, "Enhancement of composite performance by hollow polyester fibers", *J. of Tex. Polymers*, vol. 2, no. 2, pp. 45-50, 2014.

[3] M. S. Sreekala, J. George, M. G. Kumaran and S. Thomas, "The mechanical performance of hybrid phenol-formaldehyde-based composites reinforced with glass and oil palm fibres", *Compos. Sci. Technol.*, vol. 62, pp. 339–353, 2002.

[4] H. Nosraty, M. Tehrani-Dehkordi, M. M. Shokrieh and G. Minak, "The effects of hybridization on the tensile and compressive properties of basalt/nylon intraply woven fabric composites", *in Proc. ATC-11*, Daegu, South Korea, 2011.

[5] A. Pegoretti, E. Fabbri, C. Migliaresi and F. Pilati, "Intraply and interply hybrid composites based on E-glass and poly (vinyl alcohol) woven fabrics: tensile and impact properties", *Polym. Int.*, vol. 53, pp. 1290–1297, 2004.

[6] R. D. S. G. Campilho, M. D. Banea, A. M. G. Pinto, L. F. M. Silva and A. M. P. deJesus, "Strength prediction of single- and double-lap joints by standard and extended finite element modeling", *Int. J. Adhesion & Adhesives*, vol. 31, pp. 363–372, 2011.

[7] H. R. Elahidoost, M. Sheikhzadeh, S. Ajeli and A. Mostashfi, "Strength analysis of seamless double layered fabric using FEM", *J. Tex. Polym.*, vol. 2, no. 1, pp. 15-18, 2014.

[8] M. Javadi-Toghchi and S. Ajeli, "Investigation into the geometrical loop effect on tensile behavior of single bar warp-knitted fabric using finite element method", *J.Tex. Polym.*, vol. 1, no. 1, pp. 31-35, 2013.

[9] A. R. Maligno, "Finite element investigations on the microstructure of composite materials", PhD Thesis, The University of Nottingham, 2007.

[10] T. Niezgoda and A. Derewonko, "Multiscale composite FEM modeling", *Procedia Eng.*, vol. 1, pp. 209–212, 2009.

[11] S. Bhaskara, R. Devireddy and S. Biswas, "Micromechanical analysis of effect of interphase on mechanical properties of kevlar fiber reinforced epoxy composites", *Int. J. Current Eng. and Technol.*, vol. 2, pp. 115-120, 2014.

[12] P. Boisse and G. Hivet, "Consistent mesoscopic mechanical behaviour model for woven composite reinforcements in biaxial tension", *Compo: Part B*, vol. 39, pp. 345–361, 2008.

[13] R. H. W. Thije, R. Akkerman and J. Hue´tink, "Large deformation simulation of anisotropic material using an updated Lagrangian finite element method", *Comput. Methods Appl. Mech. Eng*., vol. 196, pp. 3141–3150, 2007.

[14] M. J. Wilson, "Finite element analysis of glass fibre reinforced thermoplastic composites for structural automotive components", PhD Thesis, University of Nottingham, 2003.

[15] M. N. Nahas, "Analysis of nonlinear stress-strain response of laminated fiber-reinforced composites", *Fiber Sci. and Tech*., vol. 20, pp. 297-313, 1984.

[16] Z. D. Hashin, D. Bagehi and B. W. Rosen, "Nonlinear behavior of fiber composite laminates", NASA, CR-213, 1974.

[17] K. Sirijaroonchai, "A macro-scale plasticity model for high performance fiber reinforced cement composites", PhD Thesis, University of Michigan, 2009.

[18] R. M. Christensen and J. A. Rinde, "Transverse tensile characteristic of fiber composites with flexible resins: theory and test results", *Polym. Eng. and Sci.*, vol. 19, pp.506–511, 1979.

[19] D. F. Adams and D. A. Crane, "Finite element micro-mechanical analysis of unidirectional composite including longitudinal shear loading", *computers and struct.,* vol. 18, pp. 1153-1165, 1984.

[20] L. Parietti, "Micromechanical finite element model for constitutive elastoplastic analysis of unidirectional fiber-reinforced composites", Master of Science Thesis, Virginia Polytechnic Institute and State University, 1994.

[21] C. Briancon, P. Sigety and C. G'sell, "In situ study of matrix strain in carbon/resin composite materials", *Compo. Sci. and Technol.*, vol. 56, pp. 835–840, 1996.

[22] L. G. Zhao, N. A. Warrior and A. C. Long, "A thermo-viscoelastic analysis of process-induced residual stress in fibre-reinforced polymer-matrix composites", *Mater. Sci. and Eng*., vol. 452, pp. 483– 498, 2007.

[23] Y. Zhang, Z. Xia and F. Ellyin, "Nonlinear viscoelastic micromechanical analysis of fibre-reinforced polymer laminates with damage evolution", *Inter. J. of Solids and Struct.*, vol. 42, no. 2, pp. 591-604, 2005.

[24] M. Vogler, R. Rolfes and P. P. Camanho, "Modeling the inelastic deformation and fracture of polymer composites – Part I: Plasticity model", *Mech. of Mate.*, vol. 59, pp. 50–64, 2013.

[25] M. Grujicic, T. He, H. Marvi, B. A. Cheeseman and C. F. Yen, "A comparative investigation of the use aminate-level mesoscale and fracture-mechanics-enriched mesoscale composite-material models in ballistic-resistance analyses", *J. Mater. Sci.*, vol. 45, pp.3136–3150, 2010.

[26] Y. X. Zhang and H. S. Zhang "Multiscale finite element modeling of failure process of composite laminates", *Compo. Struct.*, vol. 92, no. 9, pp. 2159-2165, 2010.

[27] A, Tabiei, Y. Jiang and W. Yi, "A novel micromechanics-based plain weave fabric composite constitutive model with material nonlinear behavior", *AIAA J.,* vol. 38, 2000.

[28] ASTM Standard D.3039, "Standard test method for tensile properties of polymer matrix composite materials", 1995.

[29] M. L. A. Grac, J. R. M. Almeida and F. A. I. Darwish, "Fracture mechanisms in epoxy resin", *J. Braz. Soc. Mech. Sci.*, vol. 11, pp. 133–146, 1989.

[30] L. E. Asp, L. A. Berglund and P. Gudmundson, "Effects of a composite-like stress state on the fracture of epoxies", *Comp. Sci. and Technol*., vol. 53, pp. 27–37, 1995.

[31] ABAQUS User's Manual, ABAQUS 6.10 Documentation, 2010.

[32] T. W. Chou and T Ishikawa, "Analysis and modelling of two-dimensional fabric composites", *Text. Struct. Compos.*, vol. 3, 1989.